Optical annular resonators based on radial Bragg and photonic crystal reflectors

Jacob Scheuer and Amnon Yariv

Department of Applied Physics, 128-95, California Institute of Technology, 1200 E. California Blvd., Pasadena, CA 91125

koby@caltech.edu

http://www.its.caltech.edu/~koby/

Abstract: A ring resonator based on Bragg reflection is studied in detail. Closed form expressions for the field and dispersion curves for radial Bragg gratings and photonic crystals based resonators are derived and compared to FDTD simulations. For strong confinement, the required gratings exhibit a chirped period and a varying index profile. Small bending radii and low radiation losses are shown to be possible due to the Bragg confinement. The sensitivity of the resonator characteristics to fabrication errors is analyzed quantitatively. A mixed confinement configuration utilizing both Bragg reflection and total internal reflection is also suggested and analyzed.

OCIS codes: (230.5750) Resonators; (130.2790) Guided waves.

References and links

1. A. Yariv, "Critical Coupling and Its Control in Optical Waveguide-Ring Resonator Systems," IEEE Photonics Technol. Lett. **14**, 483-485 (2002).
2. B. E. Little, "Ultracompact Si-SiO2 microring resonator optical dropping filter," Opt. Lett. **23**, 1570-1572 (1998).
3. C. K. Madsen and J. H. Zhao, *Optical Filter Design and Analysis: A Signal Processing Approach* (Wiley-Interscience Publications, New-York 1999).
4. R. W. Boyd and J. E. Heebner, "Sensitive Disk Resonator Photonic Biosensor," Appl. Opt. **40**, 5742-5747 (2001).
5. J. Scheuer and A. Yariv, "Two-dimensional optical ring resonators based on radial Bragg resonance," Opt. Lett. **28**, 1528-1530 (2003).
6. P. Yeh and A. Yariv, "Bragg Reflection Waveguides," Opt. Commun. **19**, 427-430 (1976).
7. K. Sakoda, Optical Properties of Photonic Crystals (Springer, New-York 1999).
8. J. Scheuer and A. Yariv, "Annular Bragg-defect-mode Resonators," J. Opt. Soc. Am. B. **20** 2285-2291 (2003).
9. S. Kim, H. Ryu, H. Park, G. Kim, Y. Choi, Y. Lee and J. Kim, "Two-dimensional photonic crystal hexagonal waveguide ring laser," Appl. Phys. Lett. **81**, 2499-2501 (2002).
10. A. Yariv, "Coupled-wave formalism for optical waveguiding by transverse Bragg reflection," Opt. Lett. **27**, 936-938 (2002).
11. M. Heiblum and J. H. Harris, "Analysis of curved optical waveguides by conformal transformation," IEEE J. Quantum Electron. **QE-11**, 75-83 (1975).
12. L. Djaloshinski and M. Orenstein, "Disk and Ring Microcavity Lasers and Their Concentric Coupling," IEEE J. Quantum Electron. **35**, 737-744, 1999.

1. Introduction

The past few years have witnessed a substantial increase in research dealing with utilization of integrated annular micro-resonators. Various applications for optical communication [1-3] and sensing [4], which are based on micro-ring and micro-disk resonators, have been suggested and demonstrated.

#3169 - $15.00 US Received October 08, 2003; Revised October 13, 2003

For many applications, annular micro-resonators exhibiting compact dimensions, low loss (high Q factor) and large free spectral range (FSR) are desired. For conventional ring and disk resonators, these parameters are limited because of the employment of total internal reflection (TIR) for radial confinement. Moreover, an improvement in one of these parameters is generally at the expense of the other. The FSR, for instance, can be increased by decreasing the resonator radius and core index, which also results in higher loss per revolution, i.e., lower Q-factor. In addition, the employment of TIR also limits the maximal transverse (radial) wavenumber or, equivalently, the minimal azimuthal number and group velocity.

Recently, we proposed to radial Bragg reflectors to confine the modal field within an annular defect [5]. The resonator structure is illustrated in Fig. 1. A circumferentially guiding defect is located within a periodic medium which could consist, for example, of a Photonic Crystal (PC) or Bragg layers. This resonator may be considered as a wrapped around line defect waveguide [6-8].

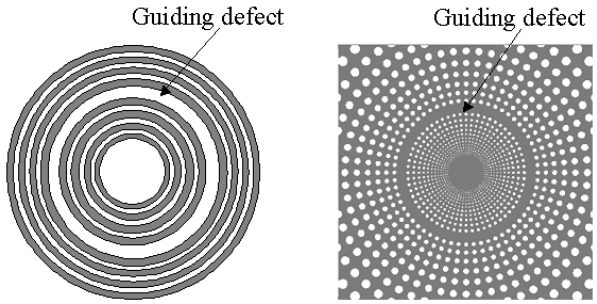

Fig. 1. A Bragg reflection based ring resonator. (A) Reflection by annular Bragg gratings; (B) Realization using an inhomogeneous hole density photonic crystal

Our structure is inherently different from the hexagonal waveguide ring resonator based on PC confinement of Ref. [9]. While our structure is radially symmetric, the structure in [9] exploited the specific symmetry of the triangular lattice to enable low loss 60° abrupt turns in order to form a closed resonator.

In order to design the annular resonator and analyze its optical properties, we take advantage of the known solution of the straight waveguide [10] and employ a conformal transformation to derive the required index profile for the annular defect resonator.

2. Resonator design

We consider the case of harmonic time behavior and of slab geometry so there are no variations in the z direction ($\partial/\partial z=0$). The modal electric field polarized in the z direction (TE) satisfies the Helmholtz equation which, in cylindrical coordinates, is given by:

$$\frac{1}{\rho}\frac{\partial}{\partial\rho}\left(\rho\frac{\partial E}{\partial\rho}\right)+\frac{1}{\rho^2}\frac{\partial^2 E}{\partial\theta^2}+k_0^2 n^2(\rho)E=0 \tag{1}$$

where ρ and θ are the radial and azimuthal coordinates respectively and k_0 is the wavenumber in vacuum. In order to transform the annular waveguide to a straight one, we utilize the following conformal transformation [11]:

$$\rho = R\cdot\exp(U/R); \qquad \theta = V/R \tag{2}$$

where R is an arbitrary parameter. The transformation (2) maps a circle in the real plane with radius R_0 to a straight line at $U_0=R\cdot\ln(R_0/R)$. Thus, the structure in Fig. 1A is transformed into a series of straight lines. The wave equation in the (U, V) plane is obtained by transforming (1):

#3169 - $15.00 US Received October 08, 2003; Revised October 13, 2003

$$\frac{\partial^2 E}{\partial U^2}+\frac{\partial^2 E}{\partial V^2}+k_0^2 n_{eq}^2(U)E=0 \tag{3}$$

where $n_{eq}(U)=n(U)\exp(U/R)$ is the profile of the refractive index in the (U, V) plane. It is important to notice that the transformed wave equation (3) is identical to the wave equation in Cartesian coordinates. The corresponding index profile in the (U, V) plane is, however, distorted – increasing exponentially as a function of U. The inverse transformation of (2) is given by:

$$U=R\cdot\ln(\rho/R),\qquad V=\theta\cdot R,\qquad n(\rho)=n_{eq}(\rho)\cdot R/\rho \tag{4}$$

The transformation (2) maps the annular waveguide of Fig.1 into a straight waveguide in the (U, V) plane. Since the requirements for a confined straight Bragg waveguide and specifically, $n_{eq}(U)$ in the (U, V) plane are known [6, 7, 10], the refractive index profile $n(\rho)$ in the real plane can be simply found by the inverse transformation (4).

Figure 2 depicts how a Bragg waveguide in the (U, V) plane is transformed to the (ρ, θ) plane. It should be noted that the gratings in the (ρ, θ) plane are spatially "chirped" i.e., their period changes as a function of the radius ρ. In addition, the index of the gratings and their index contrast become smaller for larger ρ. This effect is caused by the $1/\rho$ factor multiplying the inverse-transformed index as shown in Eq. (4). Similarly, a line defect PC waveguide [7] can be transformed to an annular defect PC resonator.

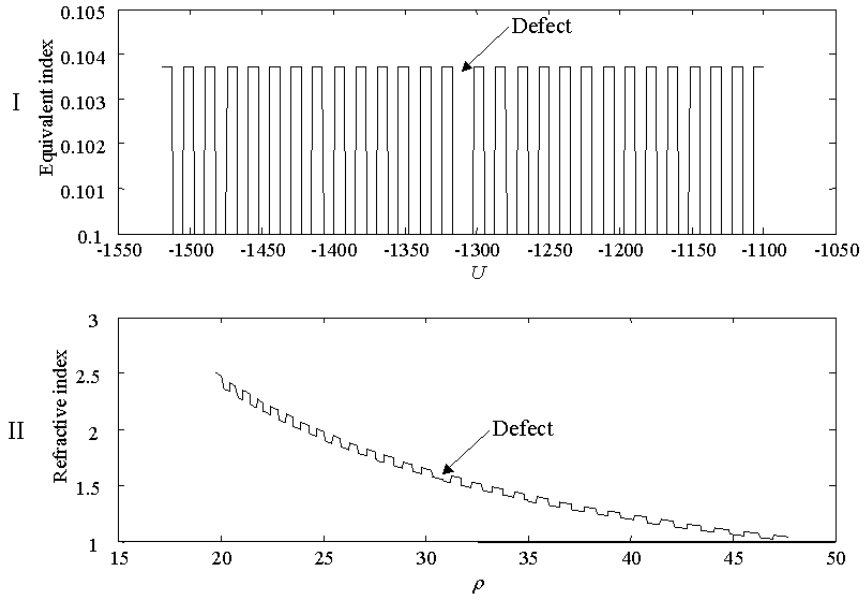

Fig. 2. Refractive index profile in (I) the (U, V) plane and (II) in the (ρ, θ) plane. R=479μm.

In order to design a Bragg resonator one has to select an appropriate line defect waveguide and a transformation radius R. This later parameter merely determines to which radius U=0 transforms to. Therefore, using different R for transforming the same line defect waveguide in the (U, V) plane result in different resonator designs in the (ρ, θ) plane. It is important to understand that the equivalent n_{eq} does not have to be larger than 1 but the real index profile, in the (ρ, θ) plane, must satisfy this requirement (see e.g., Fig 2).

#3169 - $15.00 US Received October 08, 2003; Revised October 13, 2003

3. Modal field properties

Since the modal fields of the Bragg and line defect waveguides are either known or easily calculated in the (*U, V*) plane, the field solution can be readily transformed to the (ρ, θ) plane. The guided modal solution for the transformed problem in the (*U, V*) plane is given by:

$$E(U,V) = \bar{E}(U) \cdot \exp(i\beta V) \tag{5}$$

where the propagation coefficient β can be either negative or positive, indicating a clockwise or counterclockwise propagating wave. The electric field is given by a superposition of sine and cosine functions in the defect and by Bloch waves in the gratings [6]:

$$\bar{E}(U) = \begin{cases} c_1 \cos(qU) + c_2 \sin(qU) & U_L < U < U_R \\ E_K(U) \exp(iKU) & U < U_L,\ U > U_R \end{cases} \tag{6}$$

where U_L and U_R are the left and right boundaries of the defect, $q = \sqrt{(k_0 n_{\text{defect}})^2 - \beta^2}$ and $E_K(U)$ is a periodic function of *U* with the same period as the gratings.

For small perturbation, a closed form solutions for the modal field profile and dispersion relations can be written explicitly [5]:

$$\bar{E}(U) = \begin{cases} E_0 \cos\left(\dfrac{\pi}{b}(U - U_{cent})\right) & |U - U_{cent}| \le \dfrac{W}{2} \\ E_0 \cos\left(\dfrac{\pi}{b}(U - U_{cent})\right) \exp\left[-\kappa_1\left(U - U_{cent} - \dfrac{W}{2}\right)\right] & (U - U_{cent}) \ge \dfrac{W}{2} \\ E_0 \cos\left(\dfrac{\pi}{b}(U - U_{cent})\right) \exp\left[\kappa_1\left(U - U_{cent} + \dfrac{W}{2}\right)\right] & (U - U_{cent}) \le -\dfrac{W}{2} \end{cases} \tag{7}$$

$$\beta = \sqrt{k_0^2 \varepsilon_{eq,0} - (l\pi/b)^2}; \quad l = 1,2,3... \tag{8}$$

where $\kappa_1 = 2b\left|(n_{eq}^{\max})^2 - (n_{eq}^{\min})^2\right| / \lambda^2$, U_{cent} is the coordinate of the center of the defect, $\varepsilon_{\text{eq},0}$ is the equivalent dielectric constant in the core, *W* is the defect width, *b* is the perturbation period and *l* indicates the Bragg order. $n_{eq}^{\max}$ and $n_{eq}^{\min}$ are the maximal and minimal refractive indices in the (*U, V*) plane (see e.g., Fig. 2). Unlike the equivalent waveguide, the modal field in the circular resonator $E(\rho,\theta) = \bar{E}(\rho) \cdot \exp(i\beta R\theta)$ must satisfy the cyclic boundary condition $E(\rho,\theta) = E(\rho,\theta + 2\pi)$ and, therefore, the azimuthal propagation coefficient (the phase shift per revolution) must be an integer:

$$\beta R = \sqrt{k_0^2 \cdot (n_{eq}^{\min})^2 - (l \cdot \pi/b)} \cdot R = m \qquad m = 1,2,3... \tag{9}$$

Equation (9) determines the resonance wavelengths of the structure. It is important to note that unlike conventional (i.e., TIR based) ring resonators, the dispersion relation and, therefore, the resonance wavelengths of the TM polarization are identical to those of the TE polarization.

$$\lambda_m = \frac{2 n_{\text{defect}} \rho_{\text{defect}}}{\sqrt{(m/\pi)^2 - (l/b)^2}} \tag{10}$$

where r_{defect} and n_{defect} are respectively the radius and refractive index of the resonator structure at the defect. For a given *m*, the field $E_m(\rho, \theta)$ corresponds to a mode of the resonator formed by the annular defect. The FSR of this resonator is given by:

#3169 - $15.00 US Received October 08, 2003; Revised October 13, 2003

$$FSR = \frac{d\nu}{dm} = \frac{c \cdot \sqrt{\left(2n_{eq}^{\min} \cdot \nu\right)^2 - \left(c \cdot l/b\right)^2}}{\left(2n_{eq}^{\min}\right)^2 R\pi \cdot \nu} \tag{11}$$

where c is the speed of light in vacuum and ν is the optical frequency. The FSR increases if the second term in the numerator is made as small as possible, i.e., if l=1 and b is as large as possible. If b is large enough that $\left(2n_{eq}^{\min}/\lambda\right) >> b^{-1}$ then the FSR is given by:

$$FSR \approx \frac{c}{2n_{\text{Defect}}\pi\rho_{\text{Defect}}} \tag{12}$$

It follows from (12) that the FSR increases for lower-index defect material. Unlike conventional resonators, where smaller radii require higher core index, the employment of Bragg reflectors enables high confinement of the mode in a low-index defect, regardless of the resonator radius. Therefore, a Bragg reflection based resonator is expected to have a larger FSR than that of a conventional resonator of the same radius.

Another important advantage of this structure is that its loss per revolution is determined by the Bragg structure and not by the bending radius (as in conventional ring resonators). By adding more Bragg layers to the large ρ (external) side of the defect the loss can be made arbitrarily small. In addition, because of the strong Bragg confinement, the defect can be located at any arbitrary radius.

Figure 3 depicts an FDTD simulation of a wave propagating in a line defect waveguide based on square PC (Fig. 3I) and in the corresponding annular resonator (Fig. 3II). For the line defect waveguide are lattice constant a=0.372μm, rods diameter D=0.6a, and λ=1.56μm. The rods and surroundings refractive indices are n_c=3.5 and n_s=1.5 respectively and the transformation radius is R=3.55μm. The effective index of modal field propagated in the line defect waveguide at λ=1.56μm is approximately n_{eff}=0.84 (see Fig. 3I). In order to construct a corresponding annular resonator whit that resonance wavelength, the transformation radius must satisfy the followings:

$$2\pi R k_0 n_{\text{eff}} = 2\pi m, \quad m = 1,2,3... \tag{13}$$

where m is the azimuthal wavenumber of the modal field. For different m, a different R is needed and accordingly – a different resonator structure. The modal field shown in Fig. 3II has an azimuthal wavenumber of m=12 which corresponds to a transformation radius of R=3.55μm.

In order to verify the validity and accuracy of the analysis, we employed (2) to transform the modal field profile of the line defect waveguide (Fig. 3I) to the (ρ, θ) plane and compared it with the profile of the annular resonator (Fig. 3II). Figure 4 depicts the comparison between the transformed solution (green) and the resonator modal field calculated by the FDTD simulation (blue). The match is practically perfect – indicating that the analysis method is indeed accurate.

Figure 5 shows the dispersion curve of the annular defect resonator presented in Fig. 5II. The vertical and horizontal axes indicate respectively the wavelength and the azimithal wavenumber m. The circles indicate the resonance wavelengths and the solid line represent a quadratic interpolation with the polynomial coefficients shown in the figure. The resonator FSR around 1.55μm is approximately 28nm and it increases for shorter wavelengths. The dispersion curve was calculated by an FDTD simulation of the structure shown in Fig. 3II with a short pulse (10fs) excitation.

#3169 - $15.00 US Received October 08, 2003; Revised October 13, 2003

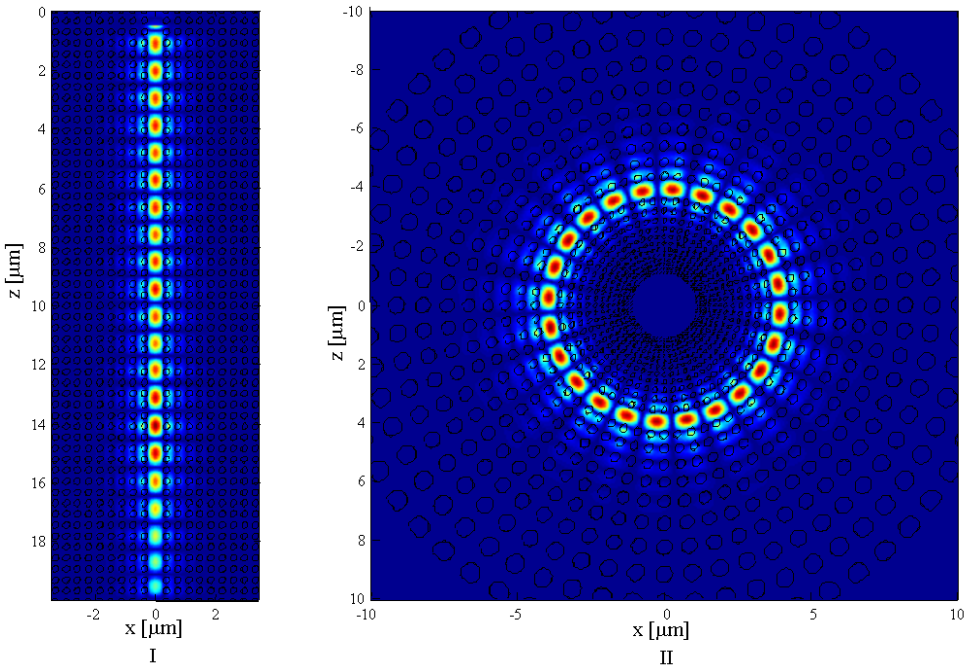

Fig. 3. Field propagation (absolute value) in I) (1.1MB) a line defect waveguide and in II) (1.5MB) the corresponding annular PC resonator.

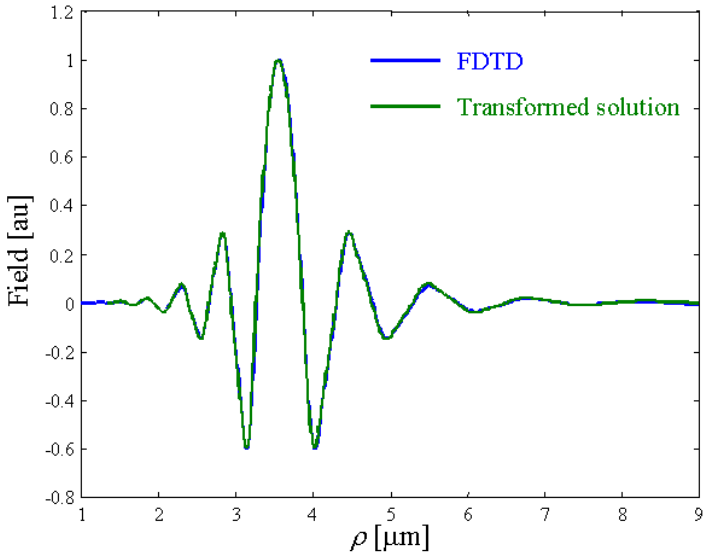

Fig. 4. Comparison between the transformed modal field profile of a line defect PC waveguide (green) and the modal field profile of the corresponding annular PC resonator (blue).

#3169 - $15.00 US
Received October 08, 2003; Revised October 13, 2003

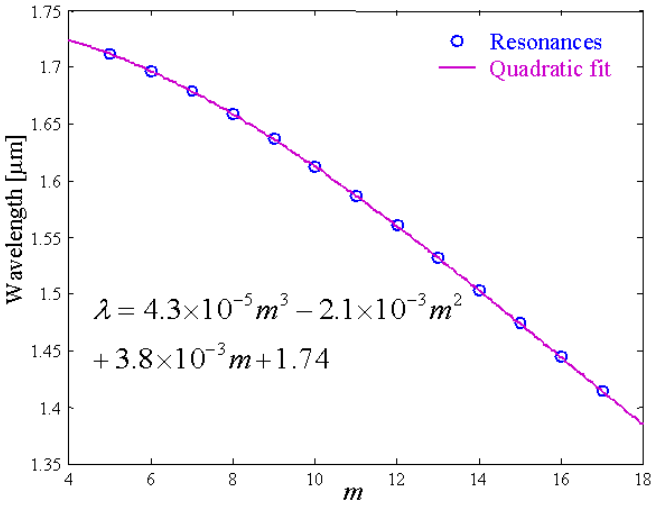

Fig. 5. Resonance wavelengths (circles) and a quadratic fit (solid line) of the resonator shown in Fig. 3II.

4. Sensitivity to fabrication errors

Ideally, the structure shown in Fig. 3II should exhibit low bending losses and large FSR. However, actual devices might incorporate small deviation from the optimal positions and radii of the holes due to fabrication errors. It is, therefore, important to examine the sensitivity of the resonators in terms of FSR, resonance wavelengths and losses (Q-factor) to such errors.

Figure 6 depicts the dispersion curves of the annular defect resonator presented in Fig. 3II, subjected to random errors in the holes positions. Each curve corresponds to accuracy tolerance on the holes position, ranging from maximal shift of 50nm (green) to 200nm (purple). The curves where calculated by an FDTD simulation of the randomly perturbed structure using with a short pulse (10fs) excitation.

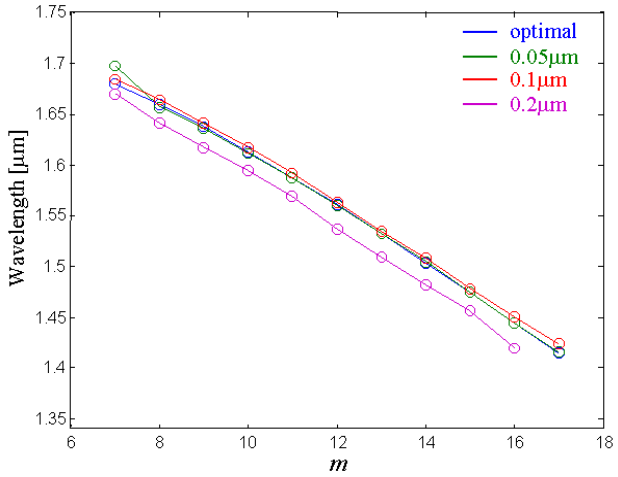

Fig. 6. Resonance wavelengths when random shifts in the holes positions are introduced: optimal structure (blue) and maximal error of 50nm (green) 100nm (blue) and 200nm (purple).

The effect of fabrication errors on the over all structure is more dominant for the lower radii regime – where the holes are small. For small deviations from the optimal holes positions (<100nm), the influence of fabrication errors, both on the resonance wavelength and Q-factor, is almost negligible. For larger errors (200nm), there is a shift of approximately

#3169 - $15.00 US Received October 08, 2003; Revised October 13, 2003

25nm in the resonance wavelengths. In addition, randomly formed local defects trap part of the field and introduce additional low-Q resonances and over-all losses to the primary modes.

Figure 7 shows the sensitivity of the dispersion curve to errors in the holes radii. As for the holes position errors, the influence of errors in the holes radii is more dominant in the lower radii regime. The holes radii were subjected to random errors with maximal error of 50nm. As can be seen in Fig. 7, the deviation of the resonance wavelength is almost negligible. However, for this type of perturbation additional low-Q resonances due to local defects appear even for 50nm perturbations.

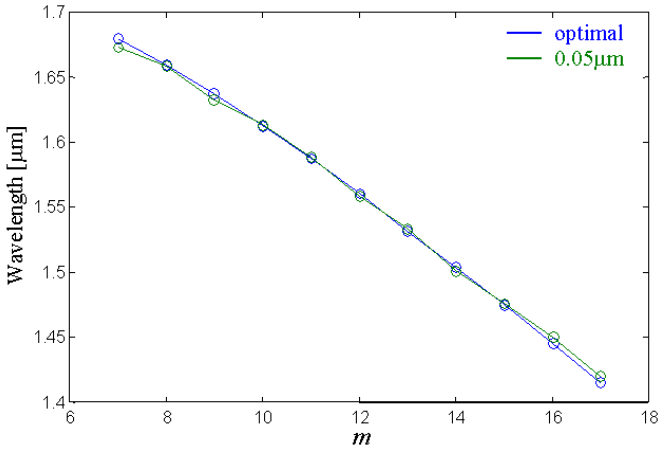

Fig. 7. Resonance wavelengths when random errors in the holes radii are introduced: optimal structure (blue) and maximal error of 50nm (green).

5. Mixed confinement methods

The index profile depicted in the upper part of Fig. 2 was chosen because it can be solved analytically. However, as can be seen in the lower part of Fig. 2, the required index in the (ρ, θ) plane might approach large values at small radii. This could be problematic because practically, refractive indices cannot be arbitrarily large. This problem, however, could be quite easily solved without sacrificing the advantages of the structure, by confining the mode on the smaller ρ (internal) side of the defect utilizing total internal reflection. A Similar approach was suggested and studied in regular (straight) Bragg waveguides [6]. It should be clear, that the confinement method of the mode on the internal side of the resonator has no effect on the resonator bending losses. Moreover, the internal side confinement is needed only for realizing a single transverse mode and for localizing the intensity in a specific radius.

Figure 8 depicts the equivalent and real index profiles of a resonator which is based on the mixed confinement-methods approach. The refractive index on the internal side of the resonator is 1.0. The electric field in the left side of the defect (inner radii) can be expressed in terms of a Bessel function of the first kind [12]:

$$\overline{E}(U < U_0 - W) = J_m(n_L k_0 R \cdot \exp(U/R)) \tag{14}$$

where n_L is the *real* refractive index on the internal side of the defect, U_0 is the coordinate of the right hand side of the waveguide (see Fig. 8I), W is the defect width and m is the Bessel order given by $m=\beta R$.

#3169 - $15.00 US Received October 08, 2003; Revised October 13, 2003

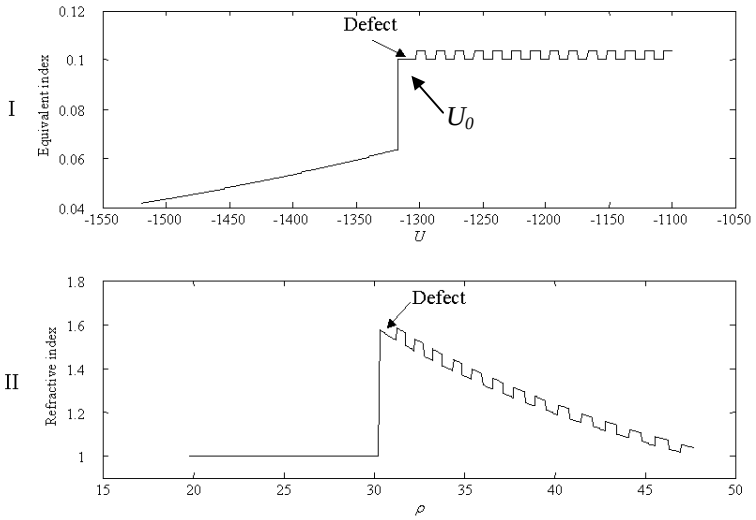

Fig. 8. Refractive index profile in (I) the (*U*, *V*) plane and (II) in the (ρ, θ) plane for a mixed confinement-methods structure. *R*=479μm.

For small perturbation, the modal field profile in the (*U*, *V*) plane is:

$$\bar{E}(U)=\begin{cases} J_m\left(n_L k_0 R\cdot\exp(U/R)\right) & U\le U_0-W \\ A_1\sin\left(\dfrac{\pi}{b}(U-U_0)\right) & U_0-W\le U\le U_0 \\ A_1\sin\left(\dfrac{\pi}{b}(U-U_0)\right)\exp\left[\kappa_1(U-U_0)\right] & U\ge U_0 \end{cases} \tag{15}$$

The characteristic equation determining the defect width *W* is found by requiring the continuity of the field and its derivative at the defect boundaries:

$$\frac{\exp\left((U_0-W)/R\right)\cdot J_m'\left(n_L k_0 R\cdot\exp\left((U_0-W)/R\right)\right)}{J_m\left(n_L k_0 R\cdot\exp\left((U_0-W)/R\right)\right)}=\frac{\lambda}{2n_L b}\cot\left(\frac{\pi W}{b}\right) \tag{16}$$

where λ is the wavelength and the prime indicates a derivative.

Although the mixed confinement-methods approach eliminates the need for very high refractive index materials it also introduces some limitations on the modal field properties. The employment of TIR instead of Bragg reflection limits, to some extent, the minimal azimuthal wavenumber of the resonator modal field which is practically confined in the defect. The reason for that limitation is that modes with lower *m* impinge on the interface with smaller angles relatively to the perpendicular. Since TIR occurs only for incident angles which are larger than the critical angle, these fields would not be totally reflected from the inner interface and, therefore, would not be confined in the defect. Nevertheless, these waves would not radiate because they would still be confined by the external Bragg reflector.

Figure 9 depicts the steady-state solution of the modal field in a resonator which employs mixed confinement-methods. The parameters of the external PC Bragg reflector are identical to those of the resonator shown in Fig. 3II. The inner radius of the defect is 3.3μm. The device was designed to have a resonance wavelength at 1.55μm and the corresponding azimuthal wavenumber is *m*=16.

Figure 10 depicts a radial cross-section of the modal field profile of the resonator shown in Fig. 9, highlighting the three different parts of field.

#3169 - $15.00 US Received October 08, 2003; Revised October 13, 2003

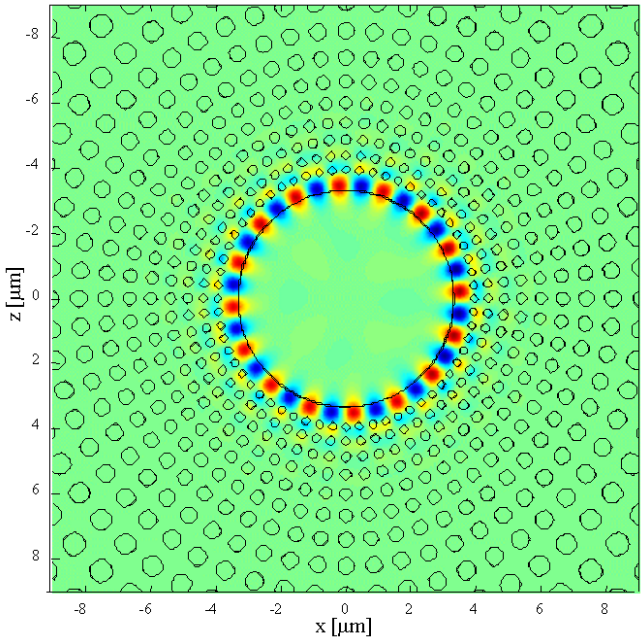

Fig. 9. FDTD simulation of an annular PC resonator employing mixed confinement-methods.

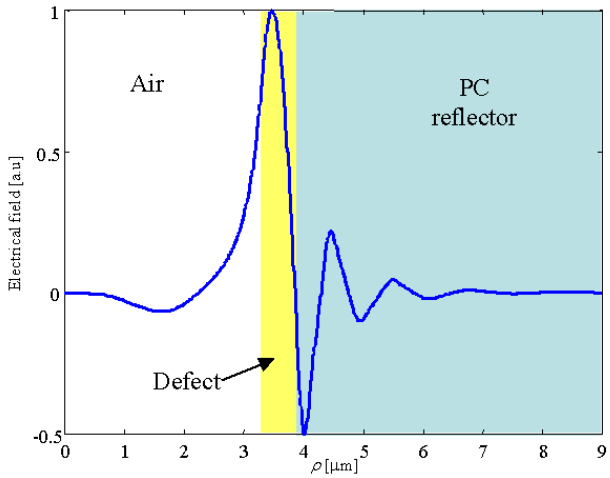

Fig. 10. Modal field profile of the resonator shown in Fig. 9.

6. Summary and conclusions

We presented an analysis a new type of annular micro-resonator which is based on Bragg reflection confinement in the radial axis. Because of the unique properties of the index profile, the micro-resonator presented here can be designed to have a very large free spectral range and low loss. By employing a conformal transformation we were able to derive the optimal refractive index profile and a closed form expression for the modal field based on the known theory of line defect waveguide. We verified our analysis by comparing a transformed modal solution of a line defect waveguide to the corresponding resonator modal field profile as calculated by FDTD simulations. To realize high radial reflection, the gratings period must be

#3169 - $15.00 US
Received October 08, 2003; Revised October 13, 2003

"chirped" – becoming longer for larger radii. In addition, the gratings' index and index contrast become larger for smaller ρ. The corresponding modal field profile exhibits similar chirped oscillations in the Bragg reflectors regime. We studied the sensitivity of the device performances to fabrication errors using the FDTD method. While small errors in the holes positions do not introduce substantial performances deviation from the optimal case, errors in the holes radii generate additional low-Q resonances because of the formation of local defects.

In order to eliminate the need for high refractive index at small radii we suggested a mixed confinement-methods approach, employing Bragg reflection for external confinement and TIR for internal confinement. This approach retains most of the properties of the dual sided Bragg resonator but its ability to confine modal fields with small azimuthal wavenumber in the defect is limited.

Acknowledgments

The authors would like to thank George T. Paloczi and Joyce K. S. Poon for helpful discussions and comments, and the reviewers for important suggestions. This research was supported by DARPA, the U.S. Office of Naval Research and the U.S. Air Force Office of Scientific Research.

#3169 - $15.00 US Received October 08, 2003; Revised October 13, 2003